SOURCE RADIATION PATTERNS IN CASED BOREHOLES

Rama Rao V. N., Roger M. Turpening, and M. Nafi Toksöz

Earth Resources Laboratory
Department of Earth, Atmospheric, and Planetary Sciences
Massachusetts Institute of Technology
Cambridge, MA 02139

ABSTRACT

Source radiation from open and cased boreholes are well documented. The effect of an unbonded casing on the radiation patterns of volume, radial stress and axial stress sources in a borehole has received less attention and is modeled and analyzed here in the context of performing single well imaging. Radiation patterns were evaluated using a global matrix approach and wavenumber integration. While a borehole with a bonded casing has a single propagating mode at low frequencies, the stoneley mode, the borehole with unbonded casing has three propagating modes. Of the two additional modes that are due to the unbonded casing, one is present mainly in the cross-section of the casing and has a phase speed close to the speed of longitudinal waves in steel. Because of its large phase speed ($\sim$ 5400 m/s), this mode radiates into almost all formations and influences the radiation pattern of all source types. Test data and the predicted radiation patterns were used to identify the annulus material behind the casing.

INTRODUCTION

A series of tests were conducted between August and October 1996 at Bayou Choctaw, Louisiana, to evaluate the efficacy of different borehole source types for performing single well imaging of salt flanks. The tests were done in a two well configuration with sources in one well (Well 15) and receivers in an adjacent well (Well 17). The two wells were 323 ft apart at the surface and 314 ft apart at a depth of 2500 ft, and 306 ft apart at 3500 ft. The salt flank was about 500 ft away from the receiver well and 300 ft from the source well, at a depth of 1000 ft. Figure 1 shows the layout of the two wells relative

to the salt dome. The sources that were tested were an airgun, an orbital vibrator and a PZT source.

This study focuses on the various aspects of wave propagation, radiation and reception in the borehole. First the physical and geometric parameters of the borehole environment were extracted from the logs of the source borehole, to construct a model. It was assumed that the receiver borehole also had similar characteristics.

We took a global matrix approach to model the radially layered borehole. The borehole modes that exist in this environment were analyzed through dispersion, attenuation and modeshapes. The borehole modes influence both the source radiation and the noise characteristics in the receivers. Hence understanding them is useful in interpreting the radiation patterns and in developing processing algorithms to eliminate borehole mode reverberation from the received signals.

We present radiation patterns of the different source types computed using wavenumber integration. These, along with the processed data from the test (Cox, 1997) are used to identify the annular material behind the casing in Well 15. The study focuses on radiation from boreholes with unbonded casings as radiation from bonded casings is well documented (Heelan, 1953; White and Sengbush, 1963; Lee and Balch, 1982; Meredith, 1990; Ben Menahem and Kostek, 1991; Meredith *et al.*, 1993).

Borehole Parameterization

The borehole parameters of the source well (Well 15) were interpreted from the logs and are given below.

Borehole Diameter

The multi-finger caliper log revealed that the casing ID was 4.95 in for the most part, corresponding well to a 5.5 in casing (15.5 lb/ft). A 30 ft segment near 3100 ft depth had an ID of 4.84 in as did all of the casing below 6200 ft. Since most of the testing was between 1500 and 4500 ft, the casing ID was assumed to be 4.95 in with a wall thickness of 0.275 in.

Cement Bond

The cement bond evaluation was done with a Segmented Bond tool (SBT). The attenuation levels of the SBT logs that were visually picked off the SBT logs had the following trend with depth.

The remarks in Table 1 are based on the log interpretation charts for the SBT where the cement compressive strengths that account for the measured attenuation are given.

This well was drilled in 1955 and very little information exists on how it was cased. It is believed that the casing from 1600–7000 ft was actually free and not cemented to the formation and that, over time, the surrounding earth closed in around the casing and raised the attenuation levels above that of the free casing. Currently, cement with a

Table 1: Cement Bonds

Depth ft	Attenuation dB/ft	Remarks
0–1600	1.75	Free pipe
1600–4700	5.25	175 psi cement
4700–7000	7	425 psi cement
7000–TD	13	3000 psi cement

Table 2: Impedances

Material	Acoustic impedance $Kg/m^3\ m/s$
Water	1.5×10^6
500 psi, 3.4 MPa, Class G/H Cement	2.8×10^6
5000 psi, 34.5 MPa, Class G/H Cement	5.8×10^6
11 lbm/gal oil-base mud	1.9×10^6
15 lbm/gal oil-base mud	2.26×10^6

compressive strength of 175 psi accounts for the attenuation in the 1600-4700 ft depth. Extrapolating from the available data on acoustic impedances of cements and muds (SBT Report), given in Table 2, 175 psi cement has an acoustic impedance close to that of water. But there was no means to ascertain if the annular material was a fluid or a solid. Hence, simulations were done assuming that the annular material was either a fluid (water) or an elastic solid, both with an acoustic impedance of 1.5×10^6 kg/m^3 m/s. The density in both cases was assumed to be 1000 kg/m^3, with a P velocity of 1500 ft and an SV velocity of 866 ft (Poisson's ratio = 0.25) for the solid. The annulus was assumed to be 0.5 in thick.

Formation

The compressional slowness in the formation was measured using a multipole array acoustic log. The formation compression speed varied between 2000 ft (150 μs/ft) and 3048 ft (100 μs/ft) over the entire well. Based on the logs, two formation models were assumed—Formation A with a compressional speed of 2200 ft, shear speed of 1270 ft and density of 2000 kg/m^3, and Formation B, with a compressional speed of 2500 ft, shear speed of 1443 ft and a density of 2000 kg/m^3.

PROPAGATION IN CASED BOREHOLES

In this section, the cased borehole is modeled and the borehole modes that exist are analyzed using dispersion, attenuation and modeshapes. These modal characteristics are useful in characterizing the modes, interpreting the radiation patterns of the borehole sources, and in modeling the pressure and displacement transients introduced in the borehole by a borehole source. The borehole source-excited transients are unwanted signals when attempting to do single well imaging; this prediction identifies the modes and their magnitudes of participation in such a scenario.

Formulation

The schematic of the model is shown in Figure 2. It has four cylindrically symmetric layers corresponding to the borehole fluid, casing, cement and formation. The annulus between the casing and the formation was modeled both as a fluid (water) and as an elastic solid. A global matrix approach is presented for the fluid annulus model. The solid annulus case was modeled using a layer matrix approach (Tubman, 1984; Tubman at al., 1986), but is not discussed here. However we show results for both cases. In the model presented, there are two fluid layers on either side of the casing. They will be referred to as the borehole fluid (inner fluid layer) and the annular fluid.

The fluids are assumed to be inviscid and the solids are assumed to be elastic and isotropic. The fluids and solids are assumed to be lossless. Axisymmetric solutions are considered. In a cylindrical coordinate system the potentials in the various layers satisfy the wave equation (White 1983),

$$\begin{aligned} \frac{\partial^2\Phi_j}{\partial r^2} + \frac{1}{r}\frac{\partial\Phi_j}{\partial r} + \frac{\partial^2\Phi_j}{\partial z^2} &= \frac{1}{\alpha_j^2}\frac{\partial^2\Phi_j}{\partial t^2}\,, \\ \frac{\partial^2\Psi_j}{\partial r^2} + \frac{1}{r}\frac{\partial\Psi_j}{\partial r} - \frac{\Psi_j}{r^2} + \frac{\partial^2\Psi_j}{\partial z^2} &= \frac{1}{\beta_j^2}\frac{\partial^2\Psi_j}{\partial t^2}\,, \end{aligned} \tag{1}$$

where Φ_j and Ψ_j are the compressional and shear potentials in the layer j and α_j and β_j are the compressional and shear speeds in that layer. The subscripts j are 1 for the borehole fluid, 2 for the casing, 3 for the annular fluid, and 4 for the formation.

Axisymmetric wave propagation in the axial direction ($\sim\ e^{-\imath kz+\imath\omega t}$) and the radiation condition that says energy only radiates outward, give the following set of solutions (White, 1983; Lee and Balch, 1982).

$$\begin{aligned} \bar{\Phi}_1(r,z,\omega) &= \int_{-\infty}^{\infty} A_1\, I_0(lr)\, e^{-\imath kz}\, dk + \bar{S}\,, \\ \bar{\Phi}_2(r,z,\omega) &= \int_{-\infty}^{\infty} \left[A_2\, I_0(m_\phi r) + B_2\, K_0(m_\phi r)\right]\, e^{-\imath kz}\, dk\,, \end{aligned}$$

$$
\begin{aligned}
\bar{\Psi}_2(r,z,\omega) &= \int_{-\infty}^{\infty} \left[C_2\, I_1(m_\psi r) + D_2\, K_1(m_\psi r)\right] e^{-\imath kz}\, dk\,, \\
\bar{\Phi}_3(r,z,\omega) &= \int_{-\infty}^{\infty} \left[A_3\, I_0(nr) + B_3\, K_0(nr)\right] e^{-\imath kz}\, dk\,, \\
\bar{\Phi}_4(r,z,\omega) &= \int_{-\infty}^{\infty} A_4\, K_0(p_\phi r)\, e^{-\imath kz}\, dk\,, \\
\bar{\Psi}_4(r,z,\omega) &= \int_{-\infty}^{\infty} B_4\, K_1(p_\psi r)\, e^{-\imath kz}\, dk\,,
\end{aligned} \tag{2}
$$

where I_ξ, K_ξ are modified Bessel functions of order ξ. l, m, n and p are radial wavenumbers in the inner fluid, casing, outer fluid and the formation, respectively, with ϕ and ψ being the subscripts of the compressional and shear components. The radial wavenumbers are as follows.

$$
\begin{aligned}
l &= \left\{k^2 - \frac{\omega^2}{\alpha_1^2}\right\}^{1/2}, \\
m_\phi &= \left\{k^2 - \frac{\omega^2}{\alpha_2^2}\right\}^{1/2}, \quad m_\psi = \left\{k^2 - \frac{\omega^2}{\beta_2^2}\right\}^{1/2}, \\
n &= \left\{k^2 - \frac{\omega^2}{\alpha_3^2}\right\}^{1/2}, \\
p_\phi &= \sqrt{k^2 - \frac{\omega^2}{\alpha_4^2}}, \quad \text{if } k \geq \frac{\omega}{\alpha_4}\,, \\
&= \imath\sqrt{\frac{\omega^2}{\alpha_4^2} - k^2}, \quad \text{if } k < \frac{\omega}{\alpha_4}, \\
p_\psi &= \sqrt{k^2 - \frac{\omega^2}{\beta_4^2}}, \quad \text{if } k \geq \frac{\omega}{\beta_4}\,, \\
&= \imath\sqrt{\frac{\omega^2}{\beta_4^2} - k^2}, \quad \text{if } k < \frac{\omega}{\beta_4},
\end{aligned} \tag{3}
$$

where the square root symbol signifies the root with positive real part. The square roots defining the radial wavenumbers introduce branch cuts and the appropriate sign convention is given above. The two possible signs of the square roots correspond to incoming and outgoing waves. For the inner fluid, the casing and annulus fluid layer, the solution is the sum of an incoming and an outgoing wave and hence, either sign can be chosen. Whereas for the formation, there is only an outgoing wave and hence the given convention is used. In the source-free case, the innermost fluid layer also requires a branch cut because it is expressed solely as an outgoing solution.

$A_1(k,\omega), A_2(k,\omega)$, $B_2(k,\omega), ...B_4(k,\omega)$ are unknown coefficients and $\bar{S}$ represents the potential of a volume source in an infinite fluid medium (Lee and Balch, 1982),

$$\bar{S}(r,z,\omega) \;=\; \frac{-V_0}{4\pi^2}\int_{-\infty}^{\infty} K_0(lr)\, e^{-\imath kz}\, dk \tag{4}$$

where V_0 is the volume displacement of the source. For the case of the volume source, the inner fluid potential $\bar{\Phi}_1$ is expressed as a sum of two potentials— one for the source in an infinite fluid medium and another which accounts for the effects of the boundary at $r = a$. The radial and axial stress sources are introduced through boundary conditions at $r = a$.

Boundary Conditions

Three boundary conditions at each of the three-layer interfaces specify the nine unknown coefficients which define the various potentials. The conditions are the continuity of radial displacement, continuity of radial stress, and the vanishing of shear stress at the inner and outer radius of the pipe and the inner radius of the borehole. Once the displacements and stresses are expressed in terms of the potentials (White, 1983), the three boundary conditions can be imposed at each of the three radial locations. The resulting equations assembled in a global matrix form are as follows.

$$[\Xi(k,w)]\{\Upsilon(k,w)\} = \{\mathcal{F}(\bar{S},k,w)\}, \tag{5}$$

where $[\Xi(k,w)]$ is a 9x9 matrix with 36 non-zero elements, $\{\Upsilon(k,w)\}$ is the vector of unknown potential coefficients $\{A_1, A_2, B_2, ...\}^T$ and $\{\mathcal{F}(\bar{S},k,w)\}$ is a vector with terms involving the source. The terms of the matrix Ξ and those of the vector $\{\mathcal{F}(\bar{S},k,w)\}$ in Eq. (5) are given in the appendix.

Dispersion

The eigenvalues are obtained as roots of the characteristic equation

$$Det[\Xi(k,w)] = 0\ . \tag{6}$$

The migration of the roots k^* in the frequency-wavenumber plane gives the dispersion characteristics of the various modes. This is obtained by solving for the roots of the above equation at different frequencies. Modes that have phase speeds less than the slowest medium speed correspond to real wavenumber roots. Those which have phase speeds that are greater correspond to complex roots. Muller's root finding algorithm (Press *et al.*, 1992) was used to locate the roots.

The various physical and geometric parameters are given in Table 3 and Table 4. The motivation for these values was provided in the previous section.

In an empty, fluid-filled or cased borehole, there is a single propagating mode at low frequencies (wavelengths are much larger than the borehole radius). But, when there

Table 3: Borehole and Formation specifications

j	Layer	Compression speed α_j m/s	Shear speed β_j m/s	Density ρ_j kg/m^3
1.	Borehole fluid (water)	1500		1000
2.	Casing (steel)	5900	3400	7800
3.	Annular fluid (water)	1500		1000
	Annular solid	1500	866	1000
4.	Formation A	2200	1270	2000
	Formation B	2500	1443	2000

Table 4: Dimensions

	ID *inch*	OD *inch*
Casing	4.95	5.5
Annulus	5.50	6.50

is a fluid annulus outside the casing, as in a poorly bonded casing, there are additional propagating modes (Tubman, 1984; Tubman *et al.*, 1986; Lee, 1991; Rao V. N., 1991). Specifically, there is an additional 'fluid' mode and a casing mode. Thus there are three propagating modes when the casing is poorly bonded and one when it is well bonded. The dispersion curves for a cased borehole with a solid or fluid annulus behind the casing are shown in Figure 3 as thick or thin lines, respectively. Additionally, two curves for each mode are for Formation A (solid line) and Formation B (dashed line).

When there is fluid behind the casing, there are three propagating modes. The casing mode propagates at a speed close to that of longitudinal waves in steel. It is weakly dispersive in both formations. The Stoneley mode in both formations propagates around 1400 m/s and is also weakly dispersive over the shown frequency range. It is faster than the formation shear in Formation A (shear speed 1270 m/s) but slower in Formation B (shear speed 1443 m/s SV). The annulus fluid mode is slower than the formation shear in both formations and is strongly dispersive.

The single mode in the solid annulus case is shown in the subplot corresponding to the Stoneley mode as thin lines. The dispersion behavior is similar to that when there is fluid behind the casing. In all cases, the stiffer formation led to an increase in the phase speeds of the modes.

Attenuation

The real part of the axial wavenumber gives the dispersion characteristics, while the imaginary part provides the attenuation characteristics of the modes. The attenuation for the ith mode, Γ_i, is computed in dB/1000 ft as,

$$\Gamma_i(k_i^*, \omega) = 20 \log_{10}(e^{\Im(k_i^*)304.8}) \,, \tag{7}$$

where $\Im(k_i^*)$ is the imaginary component of the axial wavenumber of the ith mode. The attenuations for the various modes are shown in Figure 4. No damping was included in the model. Hence all axial attenuation is due to radial leakage of energy into the formation. In a real borehole, damping in the various media and scattering due to inhomogeneities along the borehole would introduce additional attenuation. Modes that are subsonic relative to the formation shear speed for the shown frequencies that are unattenuated and are not shown in the plots.

In Figure 4, the top plot shows the attenuation of the casing mode in both formations. Below 1000 Hz, radiation from the casing mode is about 1 dB/ 1000 ft and not significant. As expected, radiation into the slower Formation A (solid line) is more than that into the faster Formation B (dashed line).

The bottom plot corresponds to the Stoneley mode with the thick solid line showing the attenuation in Formation A. Radiation from the Stoneley mode is very strong and is the dominant radiation from the borehole when there is fluid behind the casing. Below 1000 Hz, the radiation level when the annulus is a solid (thin solid line) is comparable to that when it is a fluid. The Stoneley mode does not radiate in Formation B because it is slower than the formation shear and is not shown in the plots. The annulus fluid mode does not radiate in both formations and is also not shown.

Thus, the Stoneley mode radiates strongly into the Formation A when surrounded by either a thin solid or fluid annulus of impedance 1.5×10^6 kg/m^3 m/s. The source radiation patterns will be strongly influenced by the radiating Stoneley mode. If the receiver borehole also has an unbonded casing, the strong Stoneley radiation will provide natural damping and reduce the Stoneley mode corruption of the receiver signals. In a single well configuration this would reduce the Stoneley noise in receivers that are far from the source.

Modeshapes

The modeshape of the Stoneley mode in the cased borehole is well documented (Cheng and Toksöz, 1981; White, 1983; Tubman 1984). It has plane wavefronts in the fluid and a decaying amplitude in the formation. The modeshapes in the case of a casing with fluid behind it are not as well known. Hence they are presented here for the two formations. Similar models have been investigated in the context of wave propagation in boreholes with drillpipes (Lee, 1991; Rao V. N., 1991).

The modeshapes in Formation A are given in Figure 5 and the modeshapes in Formation B are given in Figure 6. The axial displacement and stress modeshapes are

presented for 100, 500 and 1000 Hz. The plots show the variation of the displacements and stresses along the radius, from the axis of the borehole to twice the borehole radius. Complex modeshapes indicate phase differences in the response, across the layers at a given frequency and at a given location as frequency is changed. The phase difference between the axial and radial displacements controls the direction of the particle orbits and that between displacements and stresses controls energy flux or power flow per unit area.

In Formation A (Figure 5) the casing mode has displacements and stresses mainly in the cross-section of the casing. Axial energy in this mode is guided mainly in the casing. Since this mode radiates into the formation, the stresses and displacements have complex values, as opposed to pure real or pure imaginary values. The Stoneley mode is present dominantly in the borehole fluid with a smaller contribution in the annulus fluid. The annulus mode has a dominant response in the annulus with a small inner fluid and formation contribution. It has axial displacements that are purely real and stresses that are purely imaginary as it is a guided mode with no radial leakage.

In Formation B (Figure 6) the casing mode is unchanged. The Stoneley mode has pure real axial displacements and pure imaginary axial stresses as it is now slower than the formation shear. The annulus mode does not change significantly.

Transient response

A borehole source excites borehole modes in addition to the formation compression and shear waves. With the source in one well and the receivers in an adjacent well, as in the test, the source-excited borehole modes would reverberate in the source well, of which the supersonic modes would radiate. The radiation from this moving source mechanism could corrupt the data in the receiver well. In a single well imaging scenario, the source-excited borehole modes directly corrupt the measurements. To better understand these effects, the pressure transients in the borehole fluid and axial displacements in the casing are predicted for a volume source in a borehole with fluid behind the casing. These are the transients that would be sensed by a suspended hydrophone or a clamped geophone (axial component), respectively, in the source well.

The source was assumed to have a Gaussian spectrum centered at 400 Hz as shown in the following equation.

$$S(\omega) = e^{\frac{-(\omega - 2\pi 400)^2}{3\times 10^5}} \quad . \tag{8}$$

The volume injection of the source was assumed to be 1600 cm^3 (or 100 $inch^3$) and the borehole was assumed to be in Formation A.

Figure 7 shows the pressure transient in the borehole fluid and the axial displacement in the casing. The maximum pressure amplitude was 1.1×10^{10} Pa, while the maximum axial displacement was 0.06 m, 100 m from the source. The top plot shows that the hydrophone would only perceive the Stoneley mode, while the bottom plot shows that geophone would sense both the casing and Stoneley modes. In the top plot,

the amplitude responses of the casing and annulus modes are lower than the Stoneley mode by a factor of 100. In the bottom plot, casing and Stoneley mode responses are of comparable amplitudes. Additionally, annulus mode response is lower than the other two modes by a factor of 15.

Summary

An important consequence of a poorly-bonded casing with fluid behind it is the introduction of two additional modes. Energy introduced into the borehole will partition into the three modes and reverberate. Given a borehole in a specific formation, the relative levels of the three modes will depend on the excitation mechanism. A clamped geophone will likely measure both the casing mode and the Stoneley mode, while a hydrophone will measure the Stoneley mode alone. Borehole modeling of the type shown here can provide the propagation characteristics of the modes, which can then be used in identifying these modes in the data, post-processing their effects or in designing devices that can attenuate them. Attenuating the casing mode will be more challenging than attenuating the Stoneley mode due to the fact that the former propagates mainly in the cross section of the casing—a layer that is not easily accessed. Its responses in the inner fluid is small indicating, that damping devices in the borehole fluid would be ineffective against it.

SOURCE RADIATION PATTERNS

In this section, radiation characteristics of the three different sources in cased boreholes—volume, radial stress and axial stress source—are discussed. The radiation of the Stoneley and the casing modes discussed above strongly influence the source radiation patterns.

Radiation Pattern

Once the potential coefficients in the formation, A_4 and B_4, are computed for a given source type, the wavenumber integral needs to be evaluated to obtain formation displacements and stresses in the spatial domain. The potentials are given as,

$$\begin{aligned} \bar{\Phi}_4(r,z,\omega) &= \int_{-\infty}^{\infty} A_4\, K_0(p_\phi r)\, e^{-\imath kz}\, dk\,, \\ \bar{\Psi}_4(r,z,\omega) &= \int_{-\infty}^{\infty} B_4\, K_1(p_\psi r)\, e^{-\imath kz}\, dk\,. \end{aligned} \tag{9}$$

The displacements in the formation can be evaluated from the two potentials as,

$$\mathbf{U}_4 = \left(\frac{\partial \phi_4}{\partial r} - \frac{\partial \psi_4}{\partial z}\right)\mathbf{e}_r + \left(\frac{\partial \phi_4}{\partial z} + \frac{\partial \psi_4}{\partial r} + \frac{\psi_4}{r}\right)\mathbf{e}_z\,, \tag{10}$$

where $\mathbf{e}_r$ and $\mathbf{e}_z$ are the unit vectors in the radial and axial directions. These are displacements in cylindrical coordinates from which the divergence and curl of the displacement vector are computed to separate the P and SV contributions.

$$\nabla \cdot \mathbf{U}_4 = -A_4 \, K_0(p_\phi r) \, (k^2 - p_\phi^2) \, , \tag{11}$$

$$\nabla \times \mathbf{U}_4 = B_4 \, K_1(p_\psi r) \, (k^2 - p_\psi^2) \, \mathbf{e}_\theta \, . \tag{12}$$

In well-bonded casings and hard formations, i.e., where the Stoneley mode is slower than the formation shear, the integrals in Eq. (9) can be evaluated efficiently using the stationary phase method (Gibson, 1994; Gibson and Peng, 1994). However, it cannot be used in evaluating radiation patterns from poorly-bonded casings and slow formations, because of the presence of a pole (corresponding to the casing and/or the Stoneley mode that can radiate) along the integration path. The integral has to be calculated by other means, like the method of residues or wavenumber integration. In this study, wavenumber integration using the Fast Fourier Transform is used (Jensen *et al.*, 1994; Bouchon, 1980). The magnitude of the computed divergence and curl of the displacement vector is plotted on a logarithmic scale as $20 \log_{10}(\cdot)$. The various physical and geometric parameters are given in Tables 3 and 4.

Mach Radiation

When a borehole mode is faster than a formation wavetype (P or SV), it is supersonic and radiates energy in the corresponding wavetype as it propagates along the borehole. This radial energy leakage manifests itself as axial attenuation. The radiation of a supersonic mode is also termed as Mach radiation and happens in a specific region around the borehole (de Bruin and Huizer, 1989; Meredith, 1991).

Figure 8 shows a borehole source exciting a supersonic mode that sheds energy as it propagates axially. The radiating spherical wavefronts superpose in the formation to form a 'cone' that moves with the propagating borehole mode called the Mach cone. There is a also stationary cone of radiation emanating from the source called the complementary Mach cone. Characterizing these two cones are the Mach angle $\theta_{\rm m}$ and the complementary Mach angle $\theta_{\rm cm}$, shown in Figure 8.

$$\theta_{\rm cm} = \cos^{-1}\left(\frac{c_j}{c_f}\right) , \tag{13}$$

$$\theta_{\rm m} = \frac{\pi}{2} - \theta_{\rm cm} \, , \tag{14}$$

where c_j is the phase speed of mode j and c_f is the formation speed in shear or compression. $\theta_{\rm cm}$ is the complementary Mach angle and $\theta_{\rm m}$ is the Mach angle. They are defined separately in compression or shear depending on whether c_j is the formation compression or the shear velocity. This angle is measured from the vertical axis. The complementary Mach angle thus computed is overlaid on the radiation pattern plots

as dotted lines. Thus, there is radiation from the source itself and additional radiation from any supersonic borehole modes excited by the source. Depending on their relative magnitudes, features of one or both control the radiation into the formation.

Volume Source

The volume source is considered first, and is a model of the airgun. The volume injection is assumed to be 1600 cm^3 corresponding to 100 $inch^3$. The radiation characteristics of the volume source are examined as a function of frequency and formation and annulus properties.

Frequency

Figure 9 shows the comparison between the P and SV radiation from a cased borehole with a fluid annulus into formation A at 100 and 1000 Hz. The general features of the radiation are discussed first.

Only the casing mode is faster than the P velocity in Formation A. Consequently there is one dashed line in the P radiation patterns identifying the corresponding complementary Mach cone. Streaks of radiation parallel to the dashed line and in the region between the dashed line and vertical are due to the casing mode radiating into the formation. The radiation from the volume source itself is evident in the near horizontal direction, while that of the casing mode is confined within the complementary Mach cone. In this case, both radiation mechanisms are of comparable magnitudes and can be separately identified. This is not the case in the shear radiation, where the radiation from the Stoneley mode overwhelms the source radiation. Both the casing mode and the Stoneley mode are faster than the SV velocity of Formation A and hence there are two cones (two dashed lines) in the shear radiation plots. The Stoneley mode radiation is much stronger than the casing mode radiation and is expected from the attenuation plots (see Figure 4). This is due to the fact that the Stoneley mode communicates more effectively with the formation than the casing mode.

There are no significant differences between the radiation at 100 and 1000 Hz. The curl and divergence of the formation displacement are proportional to the square of frequency and hence account for the 40 dB increase in amplitude when the frequency is increased by a factor of ten. The Mach cones are at approximately the same angle in both plots because the phase speed of the modes that control them have not changed much with frequency. Both the casing and Stoneley modes are not very dispersive under 1000 Hz (see Figure 3). The source radiation changes with frequency if the source excitation of the formation is frequency dependent or if the propagation characteristics of the supersonic borehole modes change with frequency. Thus, borehole environments in which the supersonic modes are dispersive, are likely to cause significant changes in the radiation patterns.

Source Radiation Patterns

Annulus Properties

Figure 10 shows the radiation patterns when the annulus behind the casing is either water or an elastic solid with a compressional impedance equal to water. The surrounding formation is Formation A.

When there is water behind the casing, there are three modes in the borehole whereas there is only one mode when the annulus is solid. The Stoneley mode is common to both cases and the characteristic Mach cone is present in both cases in shear. The casing mode is present only in the fluid annulus and streaks of radiation corresponding to it are present in both compression and shear. In the solid annulus, there is a strong null around 58° to the the horizontal. Additionally, there is some near vertical compressional radiation that is absent in the fluid annulus case. These differences in compressional and shear radiation are used to identify the annulus material type of Well 15 described below. Thus the annulus material type controls the number of supersonic borehole modes and hence has a strong effect on source radiation patterns.

Formation Properties

The effect of formation on radiation is analyzed for both the fluid and solid annulus. Figure 11 shows the radiation when the annulus behind the casing is fluid and when the formation type is varied. When the formation changes from A to B, the Stoneley mode changes from being supersonic to subsonic relative to the formation shear. Consequently, the shear radiation changes from being dominated by the Stoneley mode to being characteristic of the volume source. The weak casing mode radiation is present in both formations and in both wavetypes (P and SV) as streaks at about 30° to the horizontal. There is a slight shift in this angle with the change in formation.

Figure 12 shows the radiation when the annulus behind the casing is an elastic solid and when the formation type is varied. Here the Stoneley mode is the only mode, and it radiates supersonically in shear in Formation A only. In Formation B the shear radiation is a lobe that is near vertical. The compressional radiation is similar in both formations though it is stronger in the soft formation. Given an annulus material type, the formation controls whether the Stoneley mode is subsonic or supersonic and hence has a considerable influence the radiation pattern.

Cross-Well Response

In this section the model results are compared with data to identify the annulus material type in Well 15 at Bayou Choctaw. In the test, the RMS geophone amplitude of the P wave first break window in the receiver well was computed for the airgun in the source well. This was done as a function of vertical geophone offset from the source depth to provide a measured 'radiation pattern'.

To mimic the P wave energy in the above 'radiation pattern', the dilation of the displacement vector in the formation was computed from Eq. (11). Note that this

includes the P wave energy at all times and not just the first break. The dilation was computed at the location of the receiver well (315 ft away from the borehole), for a range of vertical offsets, by performing the wavenumber integral in Eq. (9). This was done repeatedly over a range of frequencies (100–700 Hz) to obtain dilation as a function of vertical offset and frequency. The computed dilation is in the formation and does not include the effects of the receiver well.

The dominant response in the first break window was visually estimated from the time series data to be about 250 Hz. The spectrum of the geophone response, shown in Figure 13, revealed that there are peaks in the measured response at 260 and 490 Hz. It was surmised that the first break window is dominated by the 260 Hz peak with the second peak contributing to later events. At each offset, the frequency components of the computed dilation were summed. Two curves were created, one including all frequency components from 100–700 Hz (gray line) and another considering only the first peak, in the 220–310 Hz (black line) range. This was done for the solid and fluid annulus and also for a case when the formation compacts against the casing sufficiently to be in welded contact with it. This will be referred as the formation annulus. The results are shown in Figure 14 along with the measured data. The computed results were scaled so that all curves were at 90 dB for zero vertical offset.

The broadband response (in gray) is smooth in both the fluid and the solid annulus cases and does not look like the data, confirming the earlier conjecture about the first break containing contributions mainly from the 260 Hz peak. The narrow band results (in black) show more of the variations with offset that can be observed in the data. The undulations with vertical offset, in the fluid annulus case, are in part due to the radiating casing mode (refer Figure 10). In the solid annulus case, the null around 58° is the main feature and causes the dip in amplitudes near an offset of 500 ft. The prominent central peak near small offsets, the dip in amplitude near 350 and 600 ft and the peak around 450 ft, are features in the data that match the fluid annulus results better than the other two cases. *Thus, the casing in Well 15 at Bayou Choctaw is most likely surrounded by water.*

The fall-off in power with offset from the source is different for the fluid annulus (about 1 dB per 40 ft) from that of the solid and formation annulus (about 1 dB per 24 ft). The data shows that the response is not symmetric about zero offset. This is most likely due to the increase in formation speeds with depth. The model did not include any depth varying formation properties.

Radial Source

The next source type is a radial source that consists of unit radial stress applied to the inner wall of the casing over a length of 0.8 m corresponding to a downhole orbital source of length 80 cm. The radiation from a radial source in a cased borehole with a fluid annulus into Formation A is shown in Figure 16.

The compression radiation from the radial source is similar to that from the volume source. The radial source excites strong compressional radiation at near horizontal

angles, while at larger angles the radiation is controlled by the radiation from the casing mode. The shear radiation has a strong contribution from the Stoneley radiation at near vertical angles with a null separating it from the casing mode radiation. This strong null in shear differentiates the radial source from the volume source.

Axial Source

The final source type is an axial source that consists of unit axial stress applied to the inner wall of the casing over a length of 0.4 m corresponding to an axial vibrator of length 40 cm. The radiation from an axial source in a cased borehole with a fluid annulus into Formation A is shown in Figure 16.

The compression radiation is dominated by the Mach radiation from the casing mode. The Mach radiation is stronger than that due to the other sources as the axial source excites the casing directly. The excitation to the borehole fluid is weak and consequently there is a weak Stoneley mode. The shear radiation is also dominated by the casing mode radiation. This is very different from the radial or volume sources, which are dominated by the Stoneley radiation. In both compression and shear, the casing mode radiation overwhelms any source radiation effects and is a distinctive feature of this source.

Summary

The radiation from a borehole source into the formation is complicated in environments where supersonic borehole modes can be excited. The radiation has features of the source mechanism and the radiating mode with the relative levels depending on the source type, borehole and formation properties. A borehole with an unbonded casing is one scenario where there is *at least* one borehole mode (casing mode) that can radiate into all but the very hardest formations. An additional mode (Stoneley mode) has strong radiation in sufficiently soft formations. The presence of these modes can significantly alter the ability of a borehole source to illuminate a given target and a receiver array to perceive the reflections from the target. Thus, performing single well or cross-well imaging requires an accurate borehole model and a knowledge of the propagation characteristics of the possible modes.

CONCLUSIONS

We studied the effect of the borehole environment on three different sources used for geophysical imaging. The sources were a volume source, a radial stress source and an axial stress source. It was found that the presence or absence of the cement bond between the casing and the formation affected the source radiation significantly. Since the radiation of the three source types from boreholes with well-bonded casing is documented, this report focuses on the effects of the unbonded casing.

Detection of Unbonded Casings

The presence of a bonded (casing with a solid annular layer) or an unbonded casing (casing with an annular water layer) in a source borehole needs to be ascertained in order to do effective near-borehole modeling for imaging applications.

We showed that a geophone clamped to an unbonded casing had a strong casing mode arrival. This can be used as a diagnostic to detect unbonded casings when performing single well imaging. It was also shown that a hydrophone would dominantly sense only the Stoneley mode in the unbonded case. Analysis of an annular layer that was either water, or a solid with compressional impedance equal to water, showed that phase speeds of the Stoneley mode were only slightly different ($\sim$ 5 m/s) and attenuation levels below 800 Hz were identical for the two cases (see Figures 3 and 4). However, if there are significant changes in dispersion or attenuation levels of the Stoneley mode between the two cases, hydrophone data could also be used to distinguish unbonded casings.

The differences between an unbonded casing and a bonded casing could be observed through measurements in an adjacent well because of differences in the radiation patterns, where it was shown that the casing in Well 15 at Bayou Choctaw is most likely surrounded by water. This can be used to detect unbonded casings in the source well in two-well or cross-well imaging situations, when there are no geophones in the source well to detect the casing mode. It is worth noting that the differences in radiation exist mainly due to the fact that the annulus is a fluid and not because it had a low impedance. This is so because the annular solid, with which it was compared, had the same compressional impedance as the fluid.

Source Radiation

Wave propagation in a cased borehole is different from that in an uncased borehole due to the presence of casing and a cement or other annulus behind the casing. When the steel casing is well-bonded to the formation through an annular cement layer, the phase speed of the Stoneley mode is greater than that in a similar borehole that is uncased. This allows the Stoneley mode to radiate in faster formations than in the uncased case. This radiating Stoneley mode can overshadow the source radiation at early times and be the dominant feature.

In a poorly-bonded steel casing, where there are voids or water/mud behind the casing, the number of borehole modes increases from one to three. There is a casing mode, propagating at the speed of longitudinal waves in steel (5400 m/s), that radiates into almost all formations, in both compression and shear. The strength of this radiation is controlled by the source type, with it being the strongest with an axial source and weaker with a radial or a volume source. The other new mode is an annulus mode that is slower than most formations and does not radiate. The Stoneley mode is very similar to that in the well-bonded casing, with a strong Mach radiation in slow formations.

Frequency

The radiation patterns of the sources can change with frequency. When radiating borehole modes are present, dispersion can cause a change in the complementary Mach cone angle and consequently the radiation pattern. Additionally, excitation magnitudes of sources are normally frequency dependent and this changes the radiation levels with frequency. The radiation pattern of the volume source described earlier did not reveal significant change in character with frequency except for an increase in the overall radiation amplitude with increasing frequency. This was because the modes were weakly dispersive and the formation displacement response was proportional to frequency.

Formation

Formation type is a strong factor in borehole radiation. When the source is inside an unbonded casing in a hard formations, the casing mode and the source are the only mechanisms that radiate. It was shown in Figure 4 that the casing mode radiation decreased as formation stiffness increased. Thus as formations get harder, the source radiation patterns in poorly-bonded casings are likely to resemble those in well-bonded casings. In soft formations, the Stoneley and the casing modes radiate along with the source mechanism in unbonded casings.

Source Type

The different source types excite both the formation and the borehole modes differently and hence have varying capacities in illuminating targets in the formation. Furthermore, the radiation from a given source type in a specific formation is not fully characterized unless the borehole environment is also known. In the case of a borehole with an unbonded casing, the volume source and the radial source have a similar compression pattern, while the shear pattern of the radial source has a strong null that is absent in the volume source. The axial source was different from the other two sources, with its dominant casing mode radiation in both compression and shear.

ACKNOWLEDGMENTS

This work was supported by the Reservoir Delineation Consortium at the Massachusetts Institute of Technology.

REFERENCES

Atlas Wireline Services. Segmented bond tool SBT. Technical report, Western Atlas International, Houston, TX.

Ben-Menahem. A. and S. Kostek. The equivalent force system of a monopole source in a fluid-filled borehole. *Geophysics, 56*, 1477–1481, 1991.

Bouchon, M. Calculation of complete seismograms for an explosive source in a layered medium. *Geophysics, 45*, 197–203, 1980.

Cox, D. Evaluation of three borehole source tools recorded at the SIC Bayou Choctaw site Aug. through Oct. 96. Technical Report, Conoco, Inc., Houston, TX, February 1997.

de Bruin, J. A. and W. Huizer. Radiation from waves in boreholes. *Scientific Drilling, 1*, 3–10, 1989.

Gibson, R.L., Jr. Radiation from seismic sources in cased and cemented boreholes. *Geophysics, 59*, 518–533, 1994.

Gibson, R. L. Jr. and C. Peng. Low- and high-frequency radiation from seismic sources in cased boreholes. *Geophysics, 59*, 1780–1785, 1994.

Heelan, P. A. Radiation from a cylindrical source of finite length. *Geophysics, 18*, 685–696, 1953.

Jensen, F.B., W. B. Kuperman, M. B. Porter, and H. Schmidt. *Computational Ocean Acoustics*. AIP Press, Woodbury, NY, 1994.

Lee, H. Y.. Drillstring axial vibration and wave propagation in boreholes. PhD thesis, Massachusetts Institute of Technology, Cambridge, MA, 1991.

Lee, M. W. and A. H. Balch. Theoretical seismic radiation from a fluid-filled borehole. *Geophysics, 47*, 1308–1314, 1982.

Meredith, J. A.. Numerical and analytical modelling of seismic sources: The near and the far-field. PhD thesis, Massachusetts Institute of Technology, Cambridge, MA, 1990.

Meredith, J. A., M. N. Toksöz, and C. H. Cheng. Secondary shear waves from source boreholes. *Geophysical Prospecting, 41*, 287–312, 1993.

Press, P. H., S. A. Teukolsky, W. T. Vetterling, and B. P. Flannery. *Numerical Recipes in Fortran*. Cambridge University Press, Cambridge, 1992.

Rao V. N., R., Acoustic transmission through fluid-filled pipes in boreholes. Master's thesis, Massachusetts Institute of Technology, Cambridge, MA, 1991.

Tubman, K. Full Waveform Acoustic Logs in Radially Layered Boreholes. PhD thesis, Massachusetts Institute of Technology, Cambridge, MA, 1984.

Tubman, K., C. H. Cheng, S. P. Cole, and M. N. Toksöz. Synthetic full waveform acoustic logs in radially layered boreholes II - poorly bonded casing. *Geophysics, 51*, 902–913, 1986.

White, J. E. *Underground Sound: Application of Seismic Waves.* Elsevier Science Publishing Co., Inc., New York, 1983.

White, J. E. and R. L. Sengbush. Shear waves from explosive sources. *Geophysics, 28*, 1109–1119, 1963.

APPENDIX

GLOBAL MATRIX

The terms of the matrix $\Xi(k,\omega)$ are:

$$\Xi_{11} = lI_1(la)\,, \qquad \Xi_{54} = 2\imath k m_\psi I_0(m_\psi b)\,,$$
$$\Xi_{12} = \frac{k^2-m_\psi^2}{k^2+m_\psi^2} m_\phi I_1(m_\phi a)\,, \qquad \Xi_{55} = -2\imath k m_\psi K_0(m_\psi b)\,,$$
$$\Xi_{13} = -\frac{k^2-m_\psi^2}{k^2+m_\psi^2} m_\phi K_1(m_\phi a)\,, \qquad \Xi_{56} = \frac{\lambda_3}{\mu_2}(k^2-n^2)I_0(nb) - \frac{2n}{b} I_1(nb)\,,$$
$$\Xi_{21} = \frac{\lambda_1}{\mu_2}(l^2-k^2)I_0(la) + \frac{2l}{a} I_1(la)\,, \qquad \Xi_{57} = \frac{\lambda_3}{\mu_2}(k^2-n^2)K_0(nb) + \frac{2n}{b} K_1(nb)\,,$$
$$\Xi_{22} = -(k^2+m_\psi^2)I_0(m_\phi a)\,, \qquad \Xi_{62} = -2\imath k m_\phi I_1(m_\phi b)\,,$$
$$\Xi_{23} = -(k^2+m_\psi^2)K_0(m_\phi a)\,, \qquad \Xi_{63} = 2\imath k m_\phi K_1(m_\phi b)\,,$$
$$\Xi_{24} = -2\imath k m_\psi I_0(m_\psi a)\,, \qquad \Xi_{64} = (k^2+m_\psi^2)I_1(m_\psi b)\,,$$
$$\Xi_{25} = -2\imath k m_\psi K_0(m_\psi a)\,, \qquad \Xi_{65} = (k^2+m_\psi^2)K_1(m_\psi b)\,,$$
$$\Xi_{32} = -2\imath k m_\phi I_1(m_\phi a)\,, \qquad \Xi_{76} = nI_1(nc)\,,$$
$$\Xi_{33} = 2\imath k m_\phi K_1(m_\phi a)\,, \qquad \Xi_{77} = -nK_1(nc)\,,$$
$$\Xi_{34} = (k^2+m_\psi^2)I_1(m_\psi a)\,, \qquad \Xi_{78} = p_\phi K_1(p_\phi c)\,,$$
$$\Xi_{35} = (k^2+m_\psi^2)K_1(m_\psi a)\,, \qquad \Xi_{79} = -\imath k K_1(p_\psi c)\,,$$
$$\Xi_{44} = \frac{m_\psi^2-k^2}{2\imath k} I_1(m_\psi b)\,, \qquad \Xi_{86} = \frac{\lambda_3}{\mu 4}(n^2-k^2)I_0(nc) + \frac{2n}{c} I_1(nc)\,,$$
$$\Xi_{45} = \frac{m_\psi^2-k^2}{2\imath k} K_1(m_\psi b)\,, \qquad \Xi_{87} = \frac{\lambda_3}{\mu 4}(n^2-k^2)K_0(nc) - \frac{2n}{c} K_1(nc)\,,$$
$$\Xi_{46} = -nI_1(nb)\,, \qquad \Xi_{88} = -(k^2+p_\psi^2)K_0(p_\phi c)\,,$$
$$\Xi_{47} = nK_1(nb)\,, \qquad \Xi_{89} = 2\imath k p_\psi K_0(p_\psi c)\,,$$
$$\Xi_{52} = -(k^2+m_\psi^2)I_0(m_\phi b)\,, \qquad \Xi_{98} = 2\imath k p_\phi K_1(p_\phi c)\,,$$
$$\Xi_{53} = -(k^2+m_\psi^2)K_0(m_\phi b)\,, \qquad \Xi_{99} = (k^2+p_\psi^2)K_1(p_\psi c)\,,$$

and those of $\{\mathcal{F}(\bar{S},k,\omega)\}$ are:

$$\mathcal{F}_1 = \frac{-V_0}{4\pi^2} lK_1(la)\,,$$
$$\mathcal{F}_2 = \frac{-V_0}{4\pi^2}\left(\frac{\lambda_1}{\mu_2}(k^2-l^2)K_0(la) + \frac{2l}{a}K_1(la)\right). \qquad \text{(A-1)}$$

(A-2)

for the volume source and,

$$\mathcal{F}_2 = -2\frac{\sin(kL)}{k}\,, \qquad \text{(A-3)}$$

for the radial stress source and,

$$\mathcal{F}_1 = 2\imath\frac{\sin(kL)}{(k^2+m_\psi^2)}\,,$$

$$\mathcal{F}_3 = 2\frac{\sin(kL)}{k}, \tag{A-4}$$

for the axial stress source. The section of casing over which the radial and axial source stresses are imposed is assumed to be of length $2L$.

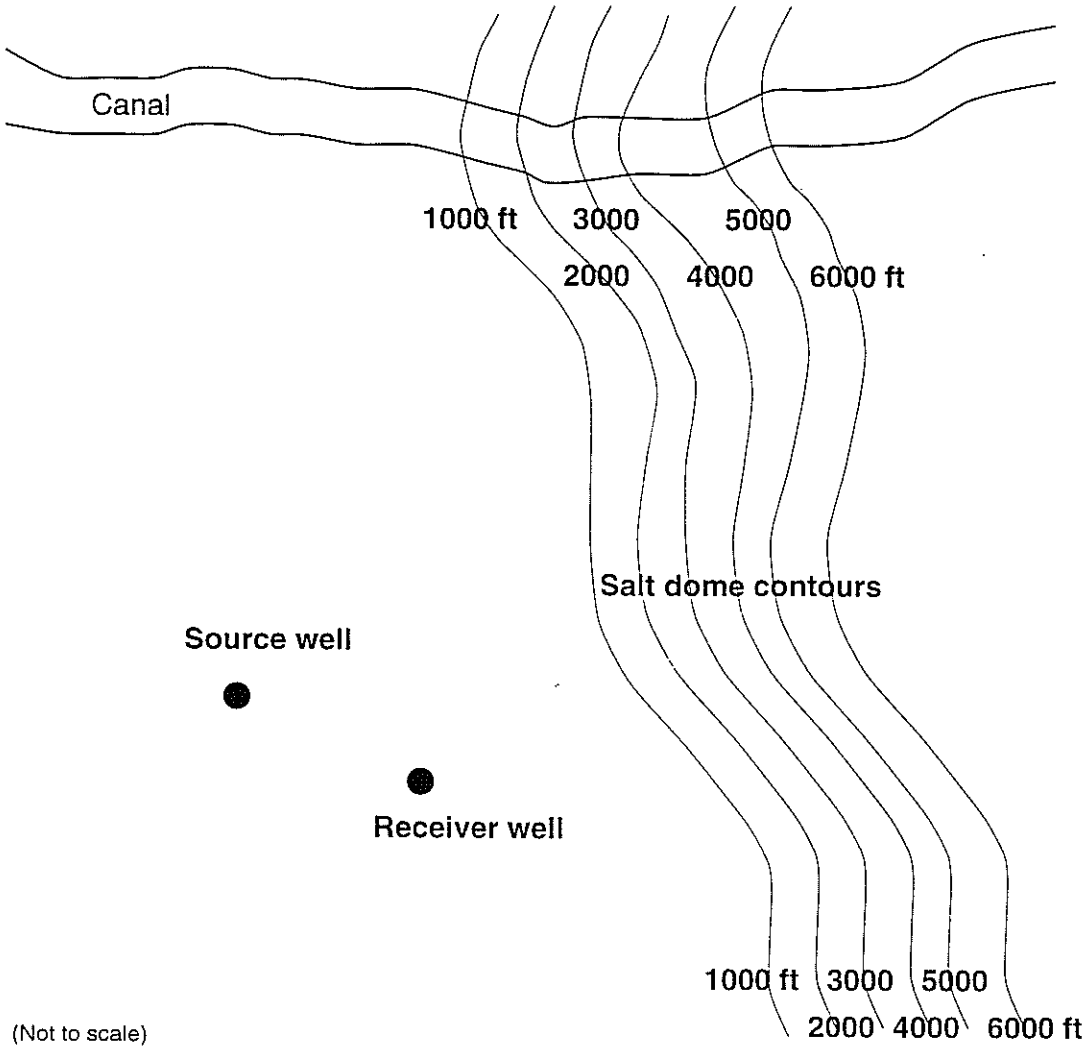

Figure 1: Layout of the source (no. 15) and receiver (no. 17) boreholes adjacent to the salt dome.

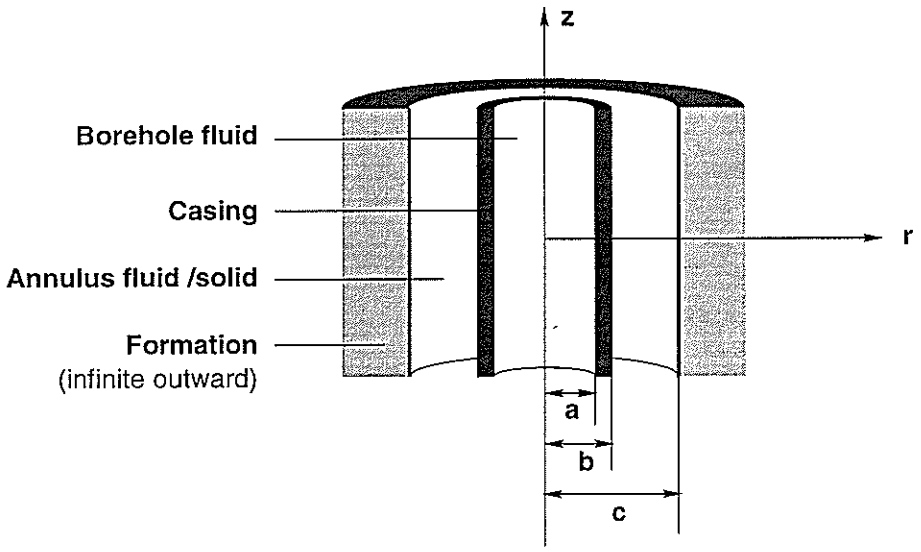

Figure 2: Schematic of a cased borehole with fluid behind the casing

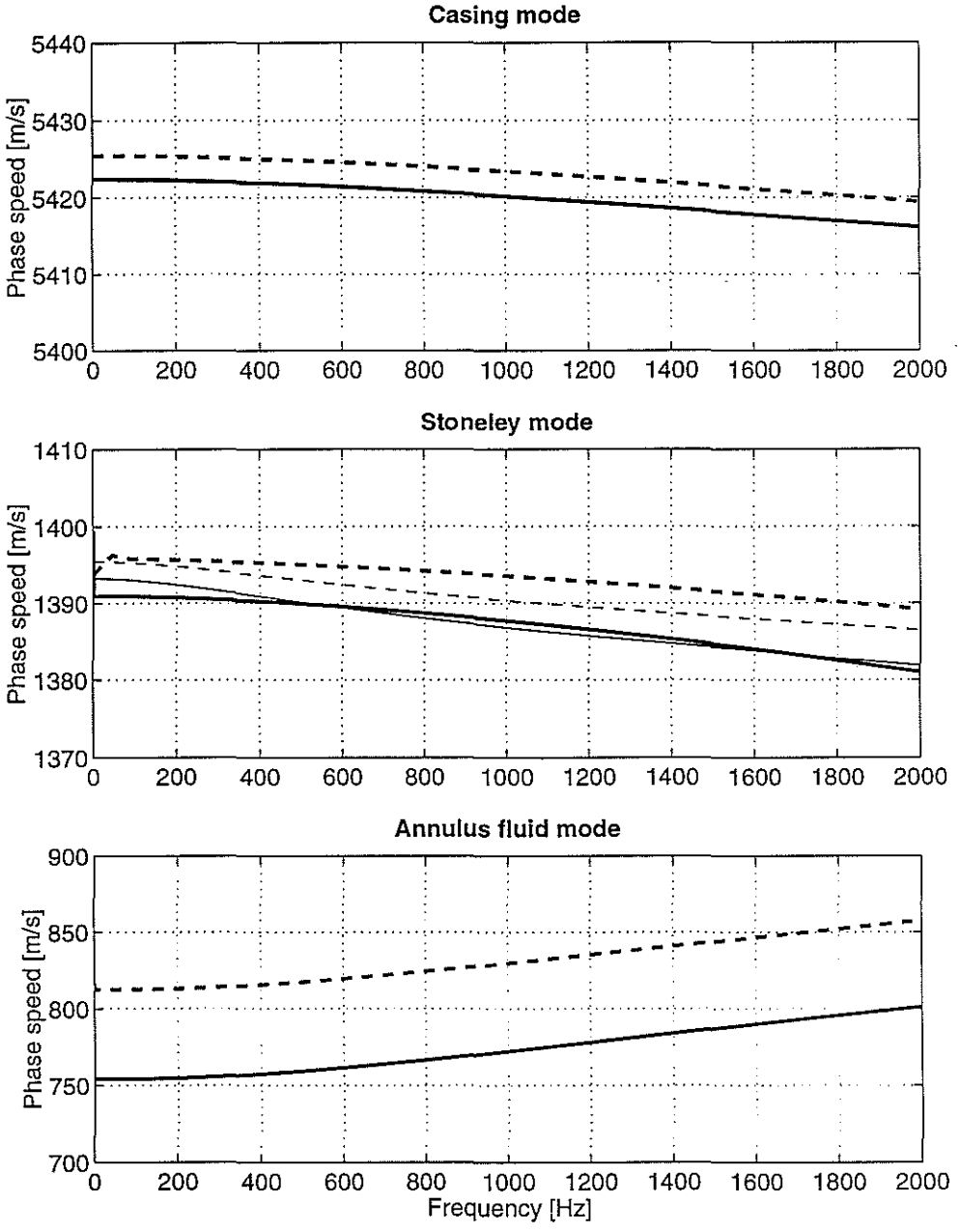

Figure 3: Dispersion characteristics of the modes in a cased borehole with a) water behind the casing, in Formation A (thick solid line), in Formation B (thick dashed line) and b) an elastic solid behind the casing, in Formation A (thin solid line) and in Formation B (thin dashed line).

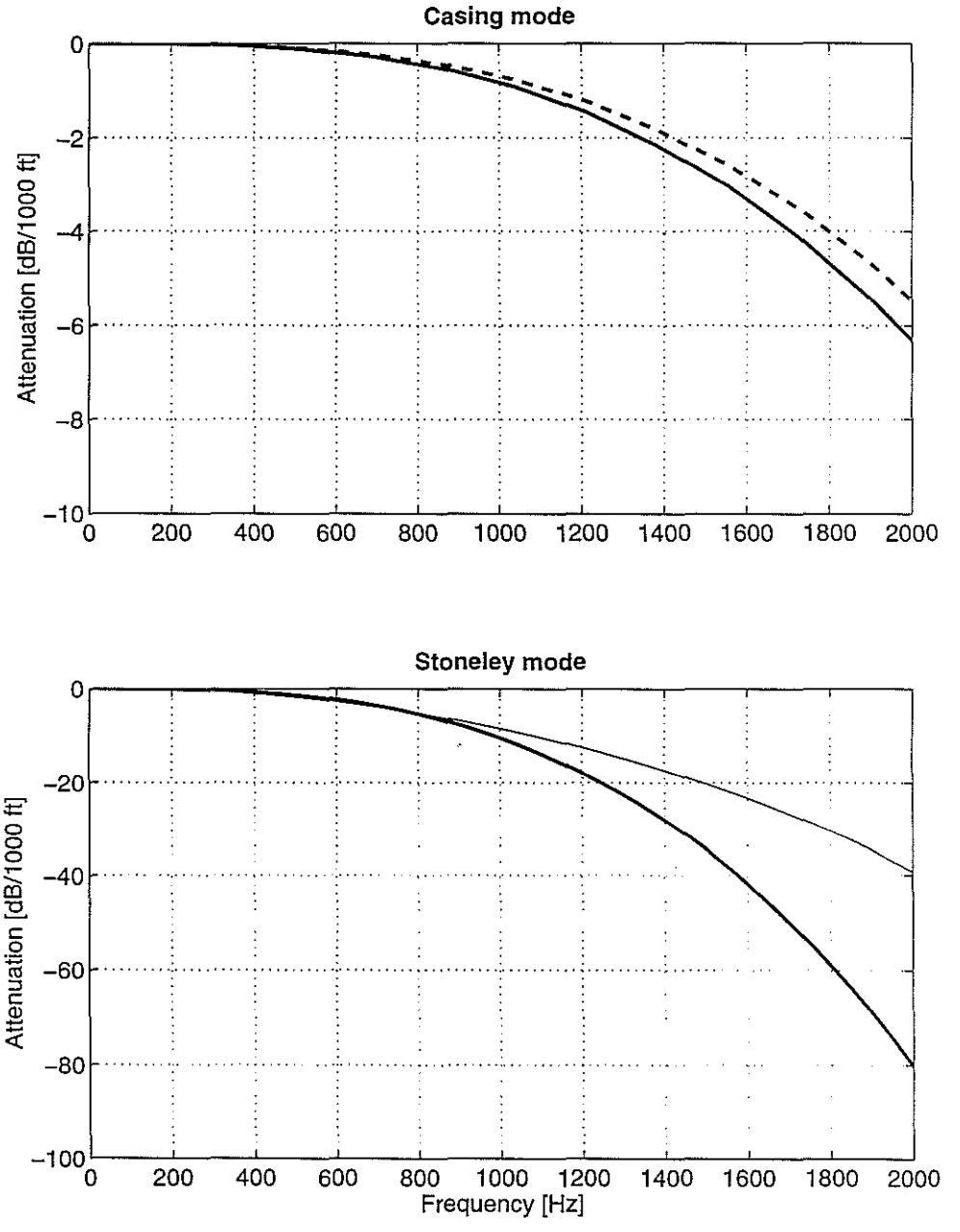

Figure 4: Attenuation characteristics of the modes in a cased borehole with a) water behind casing, in Formation A (thick solid line), in Formation B (thick dashed line) b) an elastic solid behind the casing, in Formation A (thin solid line).

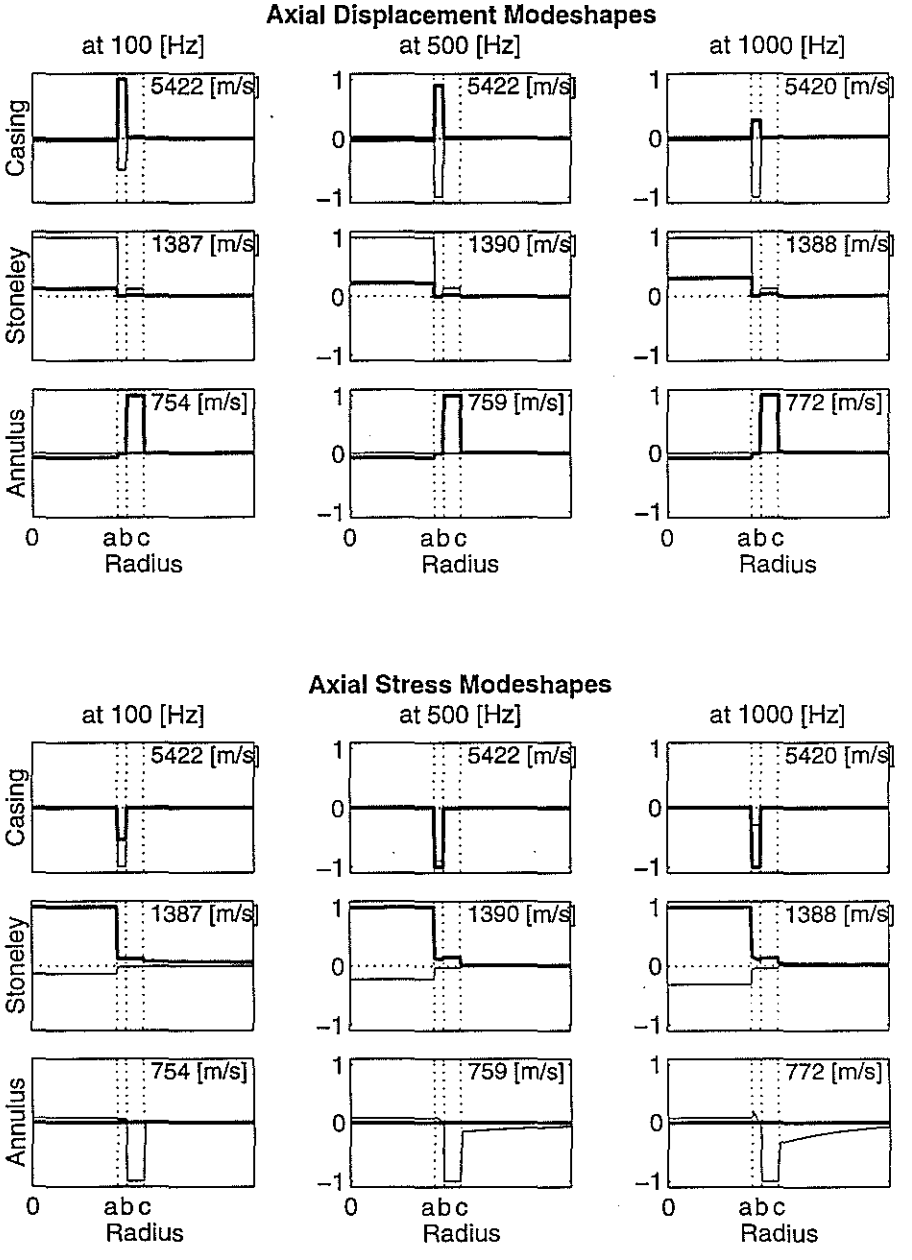

Figure 5: Modeshapes in a cased borehole with water behind casing in Formation A (P velocity 2200 [m/s], SV velocity 866 [m/s], density 2000 $[kg/m^3]$) : Real part of modeshapes (thick line), imaginary part (thin line).

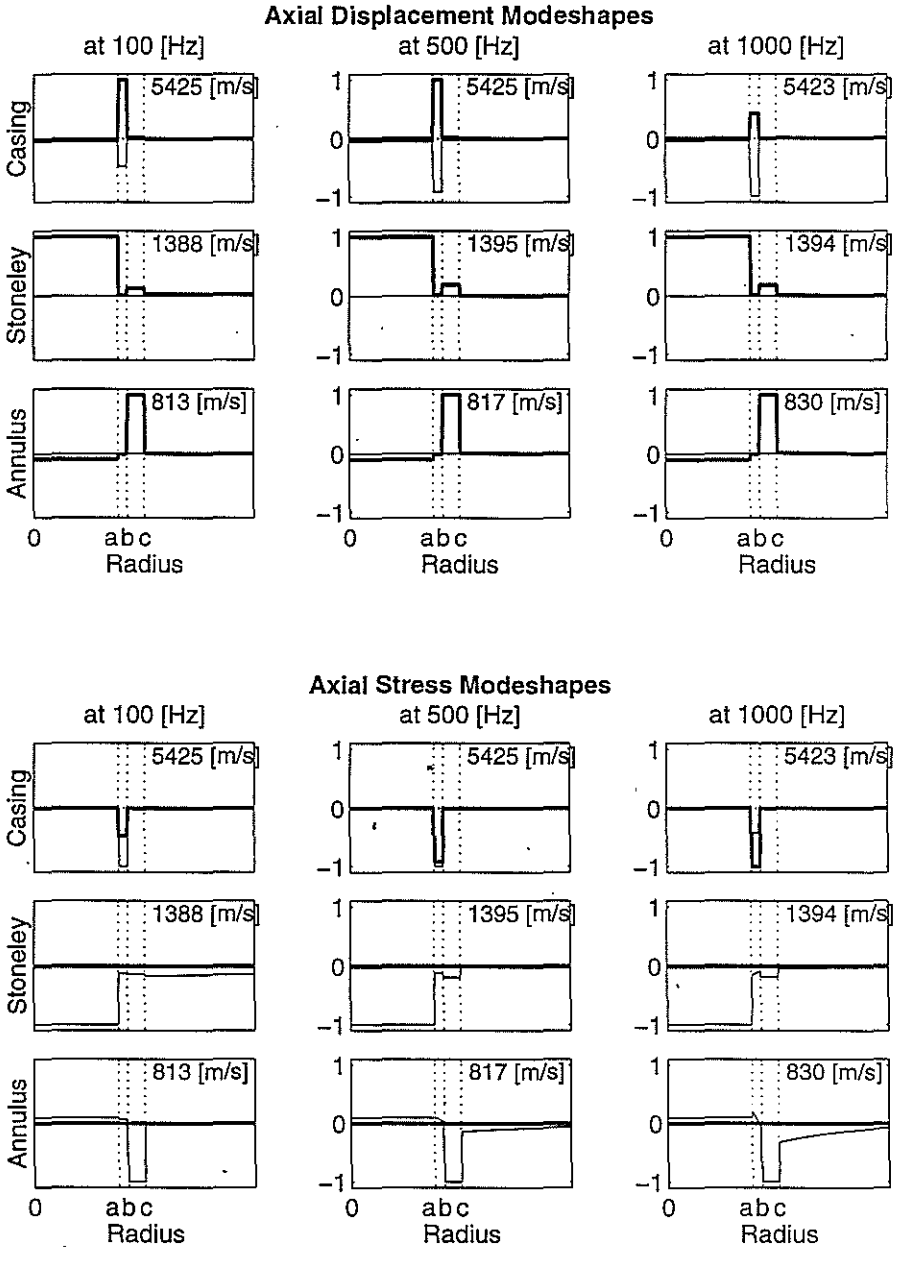

Figure 6: Modeshapes in a cased borehole with water behind casing in Formation B (P velocity 2500 [m/s], SV velocity 1443 [m/s], density 2000 $[kg/m^3]$) : Real part of modeshapes (thick line), imaginary part (thin line).

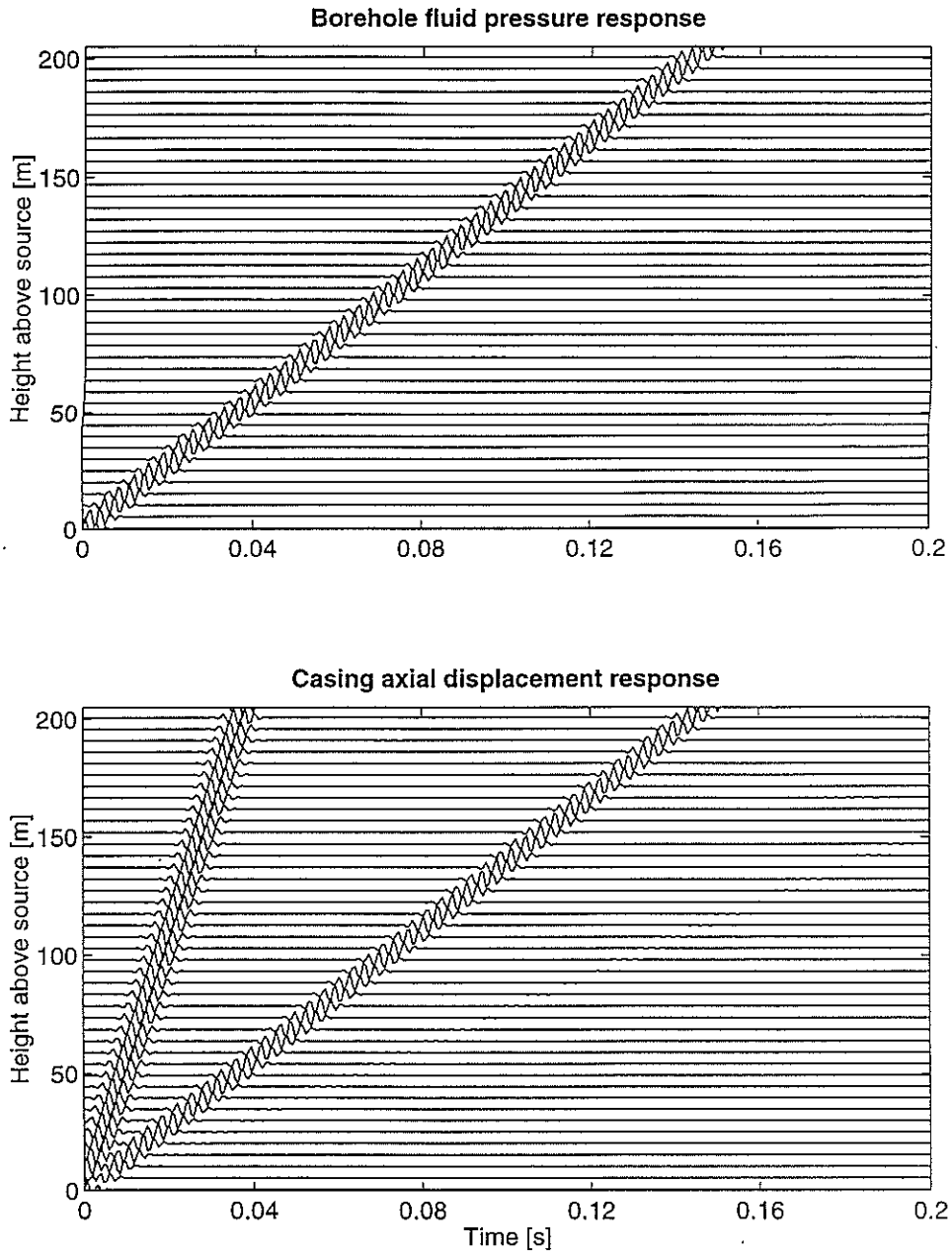

Figure 7: Top plot—Borehole fluid pressure (at r = $a/2$), bottom plot—Casing axial displacement (r = $b + 0.03$") in response to a source of volume injection of 1600 cm^3 in a cased borehole with fluid behind the casing.

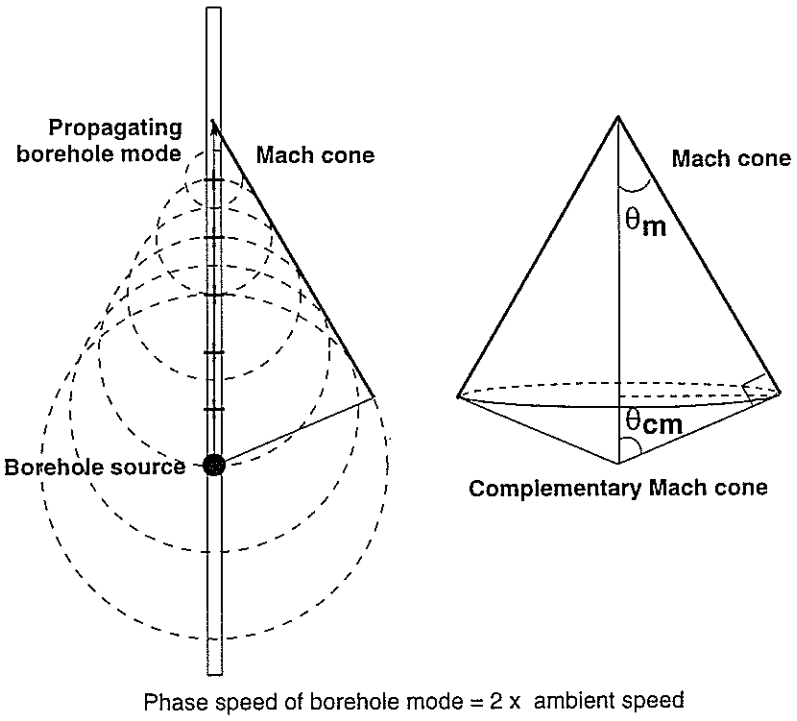

Figure 8: Mach radiation from a borehole.

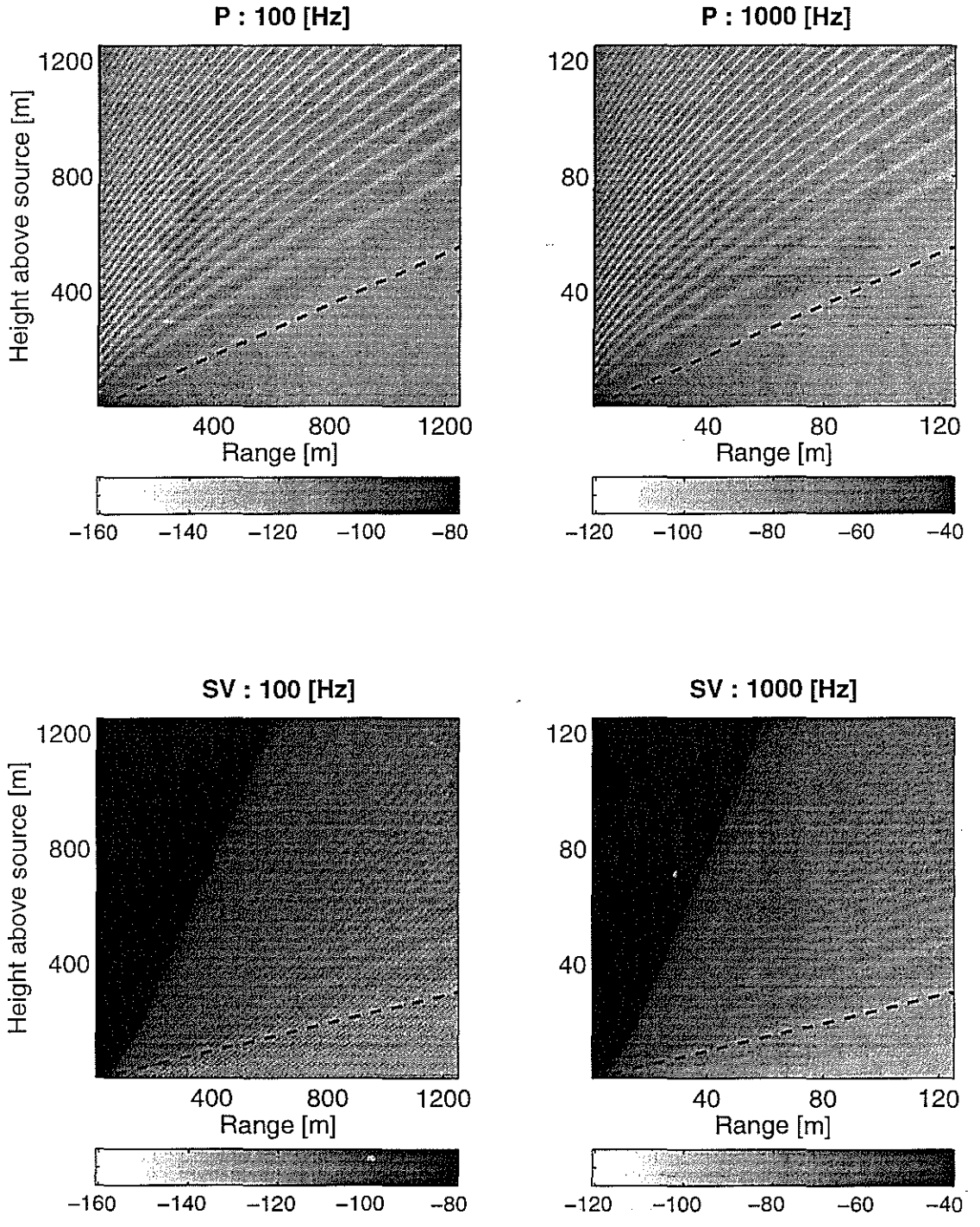

Figure 9: **Volume source**: Radiation from a cased borehole with a fluid annulus at 100 and 1000 [Hz]. Complementary Mach angle shown in dashed lines. θ_{cm} (Formation A)—casing mode in P is 66.0°, in SV is 76.5°, and Stoneley mode in SV is 24.4°.

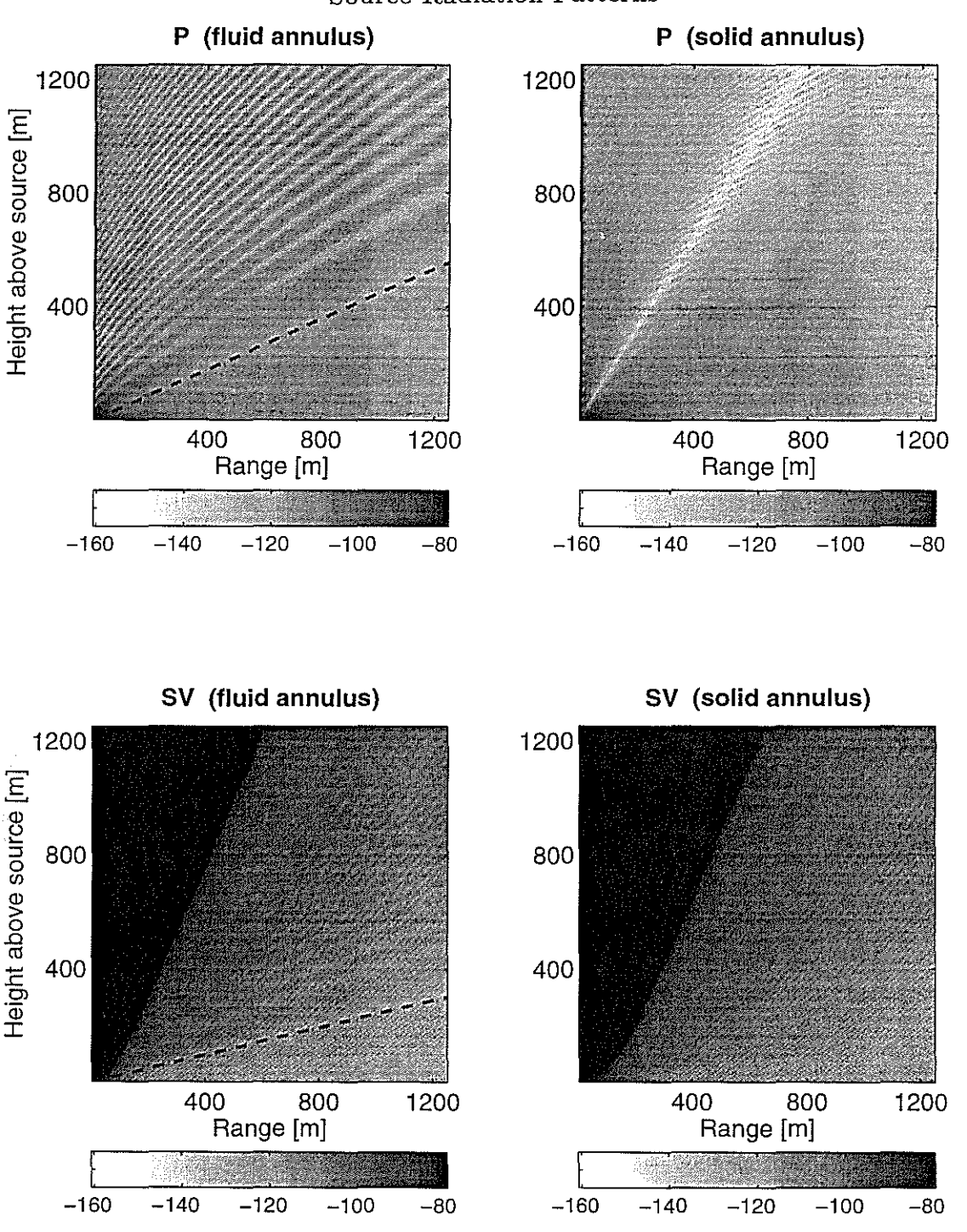

Figure 10: **Volume source**: Radiation from a cased borehole in Formation A with a fluid and solid annulus at 100 [Hz]. θ_{cm} (Formation A)—casing mode in P is 66.0°, in SV is 76.5°, and Stoneley mode in SV is 24.4°. θ_{cm} (Formation B)—Stoneley mode in SV is 24.4°.

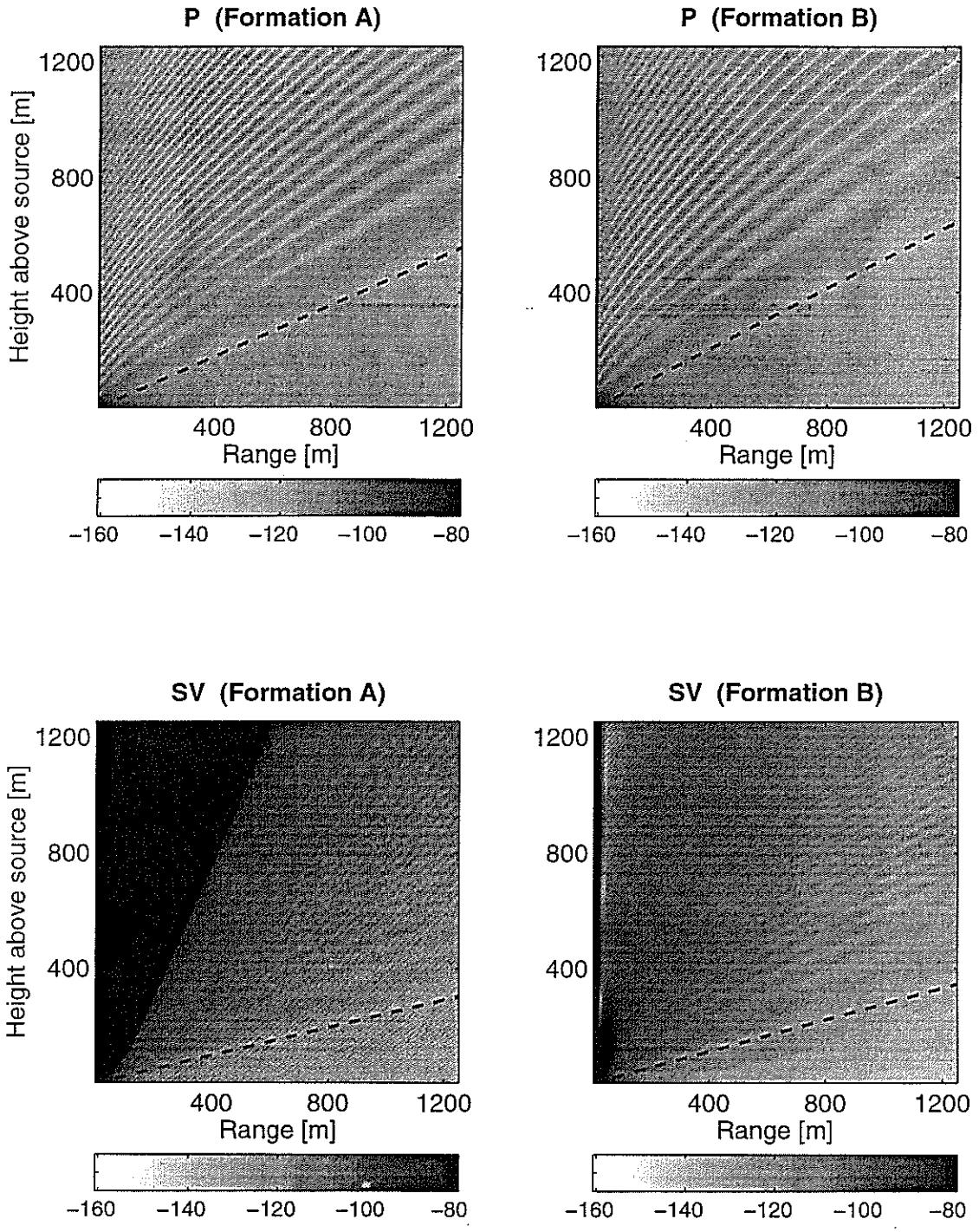

Figure 11: **Volume source**: Radiation from a cased borehole with a fluid annulus in Formation A and Formation B at 100 [Hz]. θ_{cm} (Formation A)—casing mode in P is 66.0°, in SV is 76.5°, and Stoneley mode in SV is 24.4°. θ_{cm} (Formation B)—Casing mode in P is 62.5° and in SV is 74.5°.

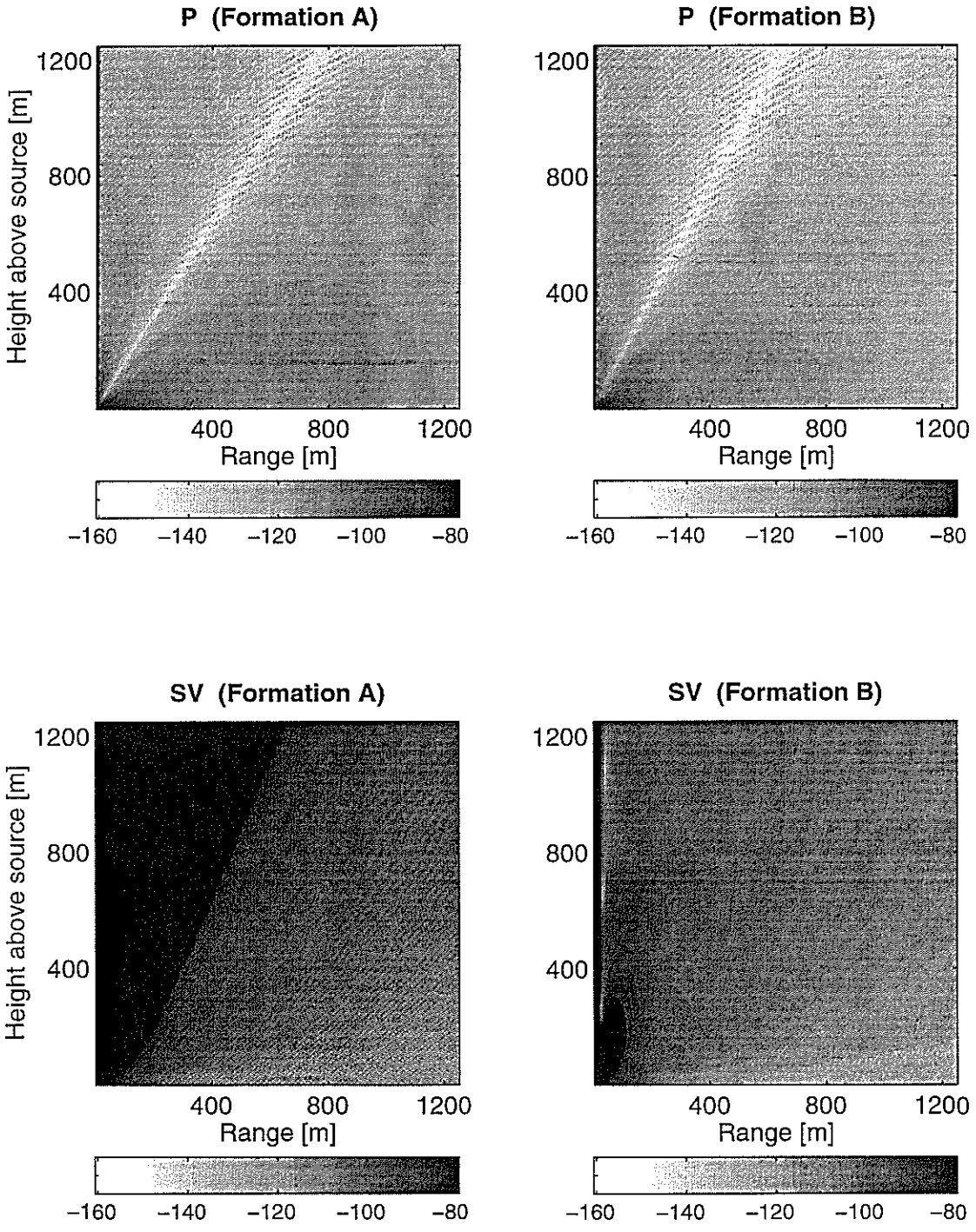

Figure 12: **Volume source**: Radiation from a cased borehole with a solid annulus in Formation A and Formation B at 100 [Hz]. θ_{cm} (Formation A) - Stoneley mode in SV is 24.4°.

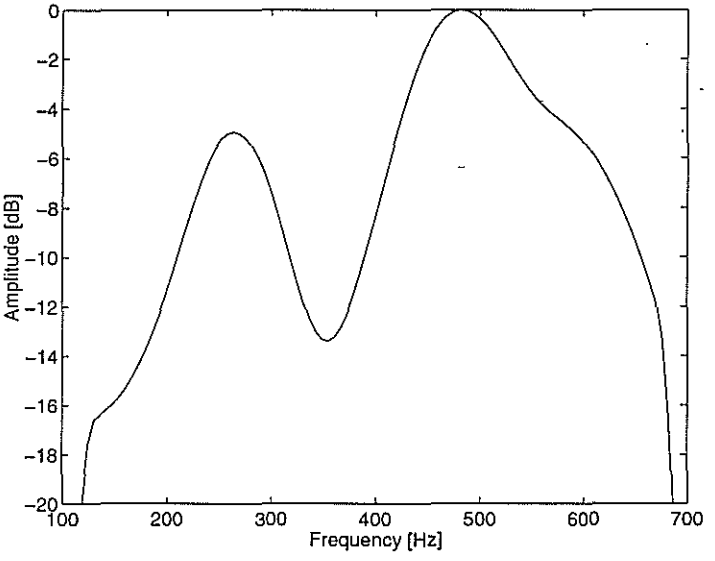

Figure 13: Measured geophone vertical component spectrum in the receiver well (Cox 1997).

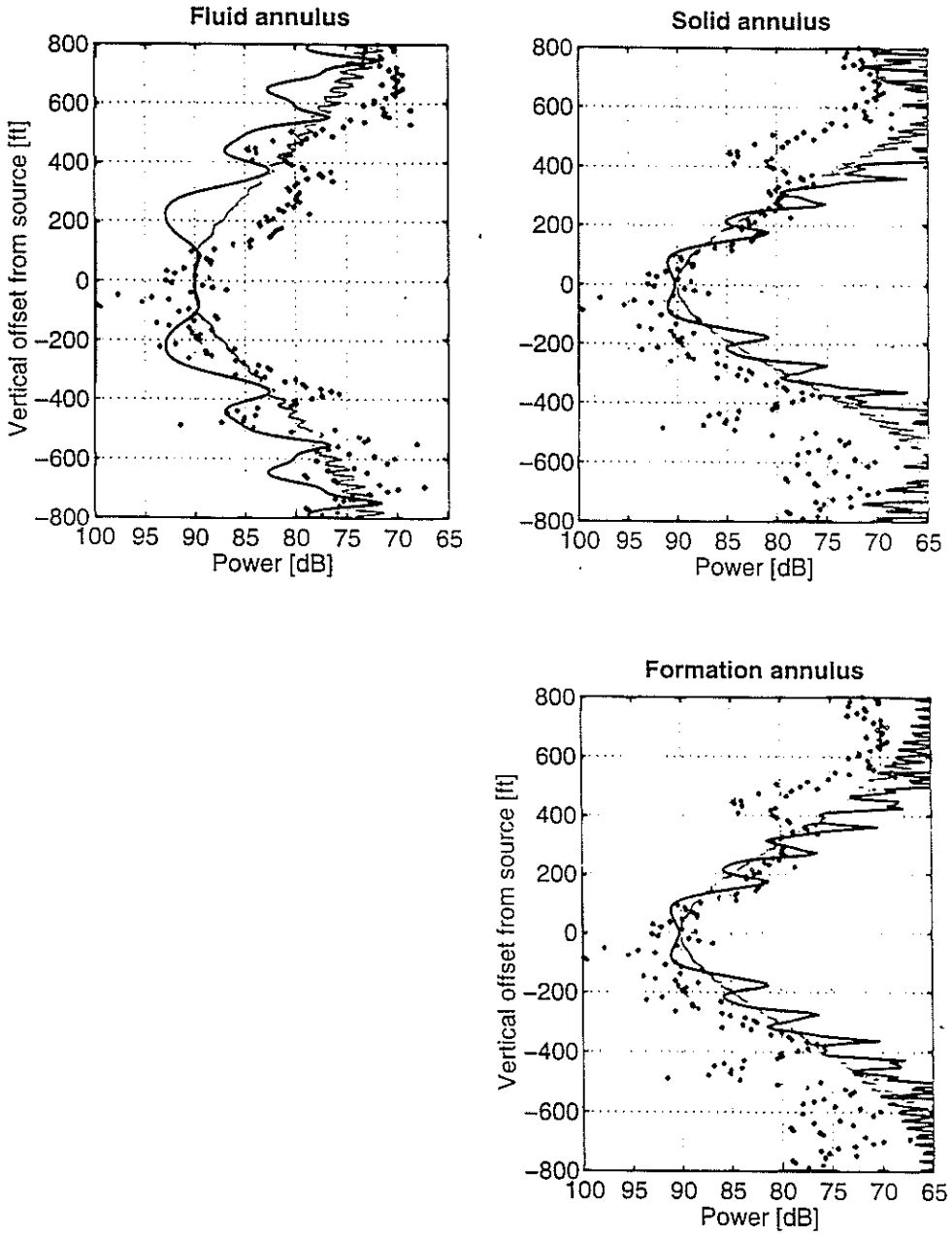

Figure 14: Comparison of RMS P first break amplitudes in the formation, at the location of the receiver well, with geophone data in the receiver well. Volume source in the source well with a fluid annulus, solid annulus or formation behind casing, radiating into Formation A. Broadband (100-700 [Hz]) result in gray and narrowband (215-325 [Hz]) result in black.

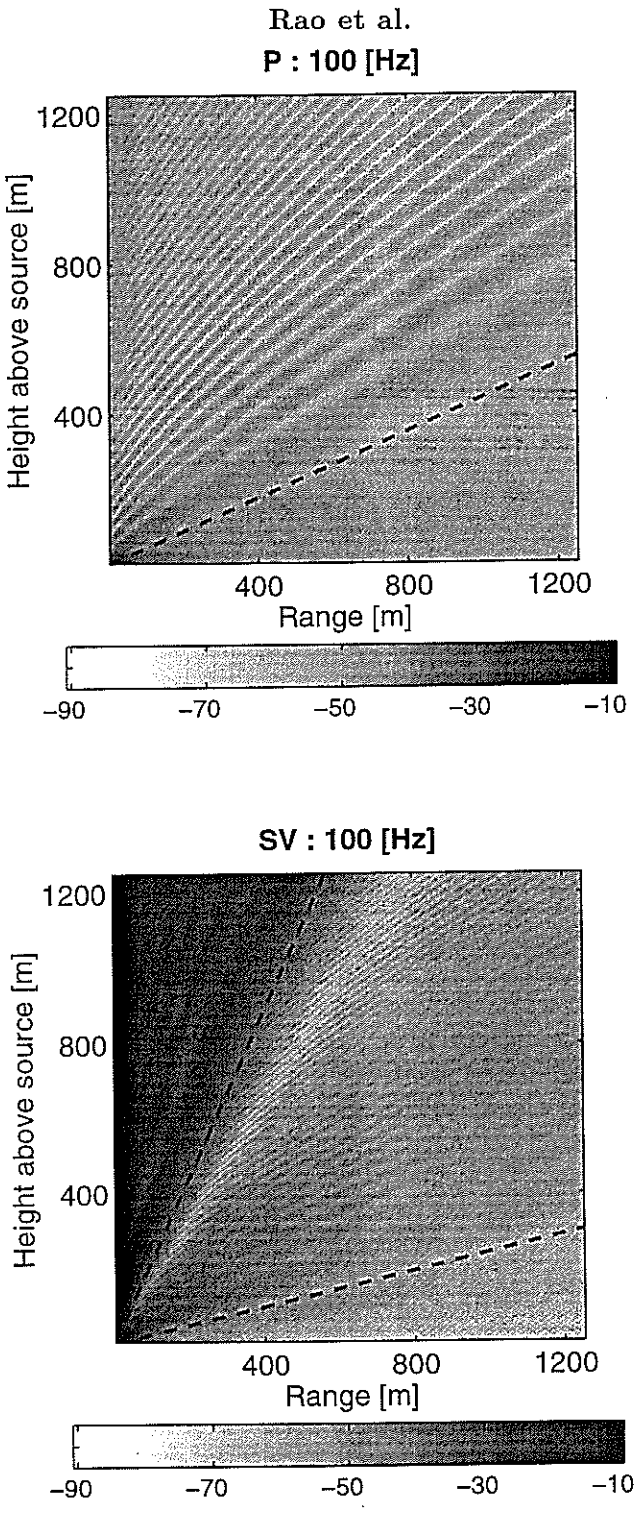

Figure 15: **Radial source**: Radiation from a cased borehole in Formation A with a fluid annulus at 100 [Hz]. Complementary Mach angle shown in dashed lines.

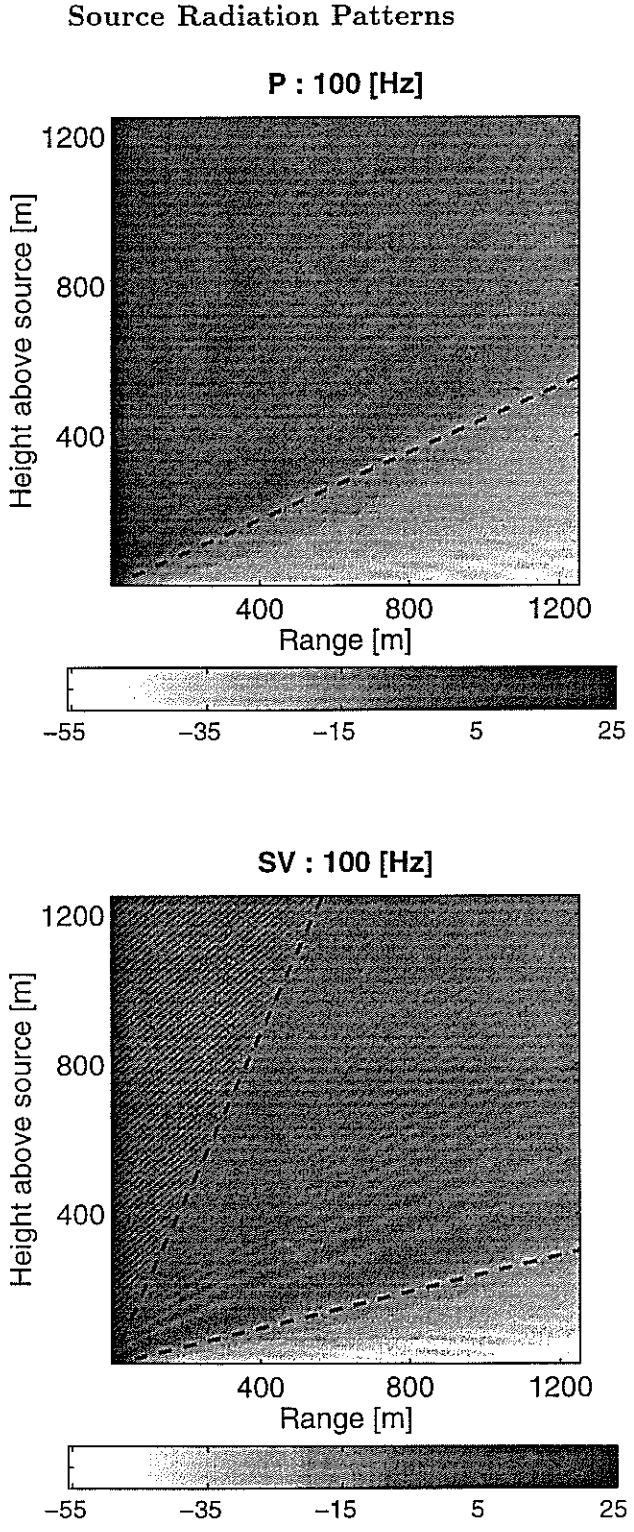

Figure 16: **Axial source**: Radiation from a cased borehole in Formation A with a fluid annulus at 100 [Hz]. Complementary mach angle shown in dashed lines.